ASSESSING TERRAIN TRAVERSABILITY OF LUNAR PSRs. H.M. Brown, P. Mahanti, M.S. Robinson, School of Earth and Space Exploration, Arizona State University; hbrown6@asu.edu

Introduction: The Moon's spin axis is tilted ~1.5° allowing for permanently shadowed regions (PSRs) within polar craters and topographic depressions, where the surface temperatures remain low enough (<100 K) to harbor frozen volatiles including water-ice [1]. Although the environment exists to trap water-ice and other volatiles, the rates of supply, burial, and excavation are unknown [2].

PSRs are thus high priority targets for future lunar exploration and possible in-situ resource extraction. However, landing and navigating a lunar rover inside a PSR presents a unique challenge that has not yet been addressed in detail. Based on the successful landings and exploration by Apollo astronauts, it is possible to compare the known traversable terrain conditions to the topography of PSRs and their associated craters, and thus evaluate exploration challenges within PSRs (given the right datasets).

In this work, we chose a total of 24 PSRs in the north and south polar regions for slope and TRI analysis using the Lunar Orbiter Laser Altimeter (LOLA) and the Lunar Reconnaissance Orbiter Camera (LROC) datasets to evaluate site accessibility.

PSR Site Selection and Previous Research: The PSRs chosen for terrain site analysis were previously identified as possible harbors for water-ice and other frozen volatiles with observations from remote sensing instruments that utilize bolometric temperature, neutron spectroscopy, radar backscatter, altimeter reflectance and the far-ultraviolet spectra [4-8].

Thermal data from Diviner revealed craters with temperatures low enough (<100K) to trap water-ice [4], and neutron counts from the Lunar Exploration Neutron Detector (LEND) led to the interpretation of enhanced hydrogen content in PSRs such as Shoemaker and Cabeus [5]. In addition, numerous PSRs show high circular polarization ratios (CPR), anomalies thought to be associated with boulder fields, impact flows, impact breccia [9, 10], or water-ice [6].

PSRs with high far-ultraviolet and near-infrared reflectance (Lyman Alpha Mapping Project (LAMP) and LOLA [7, 8]) also were used to select PSRs for this study. We characterized the traversability of the 8 largest PSRs per pole, and 8 other PSRs (24 total) were selected based on high scientific interest [4-8, 10-12] (Table 1).

Methodology: Elevation data from the gridded LOLA 30 m Digital Terrain Model (DTM) is used to compute both slope and TRI statistics, as it's the most accurate and highest resolution topographic data covering PSRs [13]. Slope and TRI statistics (median and 10th percentile values) were obtained and compared.

CRATER	PSR location (Longitude, Latitude)	PSR AREA (KM^2)	SCIENCE RATIONALE
Shoemaker	45.28, -88.03	1075	1, 2, 3, 4, 7
Haworth	357.93, -87.49	1017	1, 2, 3, 4, 7
Faustini	84.07, -87.15	664	1, 3, 4, 7
Amundsen	91.05, -83.52	439	1, 4, 7
Sverdrup	216.45, -88.25	400	1, 4, 7
Rozhdestvenskiy U	153.13, 84.55	397	1, 2, 5, 7
Wiechert J	182.61, -85.02	371	1, 4, 7
Lovelace	250.16, 81.52	339	3, 4, 7
Idel'son L	118.47, -83.89	327	4, 7
Cabeus	313.43, -84.46	315	1, 2, 4, 7
Lenard	251.75, 84.81	292	1, 4, 5, 7
Rozhdestvenskiy K	213.99, 81.82	256	4, 5, 7
Nansen F	62.47, 84.32	253	5, 7
De Gerlache	243.14, -88.31	243	1, 4, 8
Shackleton	128.20, -89.64	223	1, 3, 4
Hermite A	87.95, 307.68	211	1, 3, 5, 7
Slater	114.782, -88.10	183	1, 4, 5, 7
Sylvester N	291.34, 82.34	154	3, 5, 7
Fibiger	37.34, 86.06	120	4, 5, 7
Whipple	119.53, 89.15	87	1, 3
Hinshelwood	307.14, 89.37	60	1, 5
Un-named	337.78, -89.04	60	6, 8
Rozhdestvenskiy N	203.65, 84.02	29	3
Peary	67.74, 88.075	16	3

Table 1. Selected PSRs analyzed for terrain analysis based on size of PSR and previously identified scientific interest. Sorted by increasing to decreasing PSR size. Scientific Rationale is based on the following key: DIVINER (1), LEND (2), Mini-RF (3), LOLA (4), LAMP (5), LROC (6), size (7), and location (8).

Slope Computation. The USGS ISIS slpmap tool was used to compute slope from the LOLA 30 m DTM with an output of a 30 m/pixel slope map [14]. Slope was calculated across a 90 m baseline (3x3 pixels). To obtain slope statistics for each selected site, the slope map was then either clipped to the boundary of the PSR [15] or its associated crater wall. *Terrain Ruggedness Index*. As an alternative measure to slope,

TRI provides a means to quantify topographic heterogeneity by measuring variation about a central pixel [16]. TRI corresponding to a 3x3 grid was computed as the mean absolute difference of the central elevation value from adjacent neighbors [16]. TRI values were computed from the LOLA DTM at 30 m/pixel, using the method described above, and the resulting rasters were clipped to the PSR and crater wall boundaries.

Comparing PSR Terrain Results to Apollo Landing Sites. Lawrence et al. (2015) obtained slope and TRI measurements from LROC NAC DTMs of successful lunar landing sites at 2m/pixel to quantify known traversable lunar terrain. They identified 1 km circular Regions of Interests (RoIs) around selected sites to obtain NAC DTM slopes <10º and TRI values between 0.077 and 0.462.

In order to compare slope and TRI values between the 30 m LOLA DTM and the 2 m NAC DTMs, the 2 m DTMs were re-sampled to 30 m/pixel. Median slope values were computed for the full 30 m NAC DTMs of the landing sites, as the RoI shapes were not available. Median slopes were 2.4º - 10.6º at 2 m, and 1.3º - 10.4º at 30 m for the landing site DTMs, lending a degree of confidence to the leap from 2m DTMs to 30 m DTMs.

Average median TRI values were 0.06 – 0.52 at 2 m, and 0.00 – 0.33 at 30 m for the landing site DTMs. TRI values increase with baseline [17], hence a satisfactory value of TRI at 30 m/pixel means similar or lower values at smaller baselines, but the nature of TRI at rover scale from 30 m/pixel baseline is ambiguous. As such, we derive our conclusions from median slopes <10.4º at a baseline of 30 m, for terrain site accessibility of the selected PSRs.

Results and Discussion: The 24 PSRs in this study had an mean 10th percentile slope of 4º. The average median slope of the PSRs was 8.8º, with 19 PSRs having median slopes less than the landing sites (<10.4º). Crater walls of the PSRs had higher slopes, with the mean 10th percentile value of 8.2º, and an average median slope of 18º. None of the PSRs had median crater wall slopes <10.4º.

Slope statistics reveal that a PSR in Amundsen crater as having the lowest wall slopes (10th percentile slope 4.9º), and Slater PSR as having the lowest PSR slopes (10th percentile slope 1.3º). Slope values for PSRs such as Rozhdestvenskiy N, Shackleton, and Whipple indicate terrain that is not ideal for traversing (10th percentile slope > 10º).

Note that while average slope describes local slope statistics, the 10th percentile slope focuses on terrain units within the larger study areas of the PSRs, which can include crater floors and/or crater walls with lower slopes that may be traversable (Figure 1). On average, crater wall slopes are 5º steeper than PSRs, with the exception of Rozhdestvenskiy N, whose PSR is mostly crater walls (3:1). Though there is no definite trend between PSR area and slope, PSRs in degraded craters and topographic depressions would likely have lower slopes than PSRs in fresh craters.

Conclusions and Future Work: As illustrated, the necessity of terrain site analysis of PSRs provides a practical assessment of possible surface operations at or near sites of interest. From this very basic analysis, we conclude that for most PSRs, having a lander delivering rovers and/or humans in the PSRs minimizes risk by avoiding a traverse down steep crater walls. However, this does not preclude all PSRs from having a traversable path into the PSR.

Future work will rank PSRs based on a traversability index based on slope, scientific interest, other factors that influence mobility [18], and distance to illuminated terrain [19, 20]. We also note that a higher resolution topographic dataset of the PSRs will enable a more robust analysis.

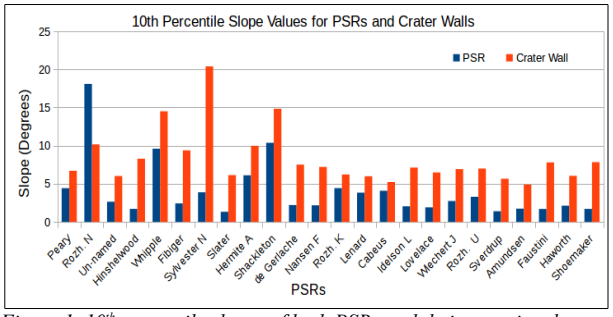

Figure 1. 10th percentile slopes of both PSRs and their associated crater walls. Sorted by PSR area (km^2) in increasing size.

References: [1] Watson et al. (1961), J. Geophys. Res., 66, 3033. [2] J.R. Arnold (1979), J. Geophys. Res., 84, 5659. [3] S.J. Lawrence et al. (2015), LPSC XLVI, abs. #2074. [4] D.A. Paige et al. (2010), 330, 6003. [5] A.B. Sanin et al. (2012), J. Geophys. Res., 117, E12 [6] P.D. Spudis et al. (2013) J. Geophys. Res., 118, 10. [7] P. Glaser et al. (2014), Icarus, 243, 78- 90. [8] G.R. Gladstone et al. (2012), J. Geophys. Res., 117, E12. [9] S.D. Koeber et al. (2014), LPSC XLV, abs. #2811. [10] Mitchell et al. (2017), LPSC XLVIII, abs. #2481. [11] P.O. Hayne et al. (2015), J. Geophys. Res., 255, 58-69. [12] A. Colaprete et al. (2010), Science, 330, 6003, 463-468. [13] D.E. Smith et al. (2010), Geophys. Res, Lett., 37, 18. [14] K.J. Becker et al. (2013), LPSC XLIV, abs. #2829. [15] E. Mazarico et al. (2011), Icarus 211.2, 1066-1081. [16] S.J. Riley et al. (1999), intermt. J. sci. 5.1-4. 23-27. [17] M. Samadrita et al. (2013), J. ESS 122.3, 869-886. [18] H. Seraji (1999), IEEE, 3. 2006-2013. [19] L. Pedersen et al. (2008), I-SAIRAS. [20] E.J. Speyerer et al. (2013), Icarus 222.1, 122-136.